PERGAMON

Journal of Quantitative Spectroscopy & Radiative Transfer 68 (2001) 419–433

Journal of Quantitative Spectroscopy & Radiative Transfer

www.elsevier.com/locate/jqsrt

Submillimeter atmospheric transmission measurements on Mauna Kea during extremely dry El Niño conditions: implications for broadband opacity contributions

J.R. Pardo[a,*], E. Serabyn[a], J. Cernicharo[b]

[a]*George W Downs Laboratory of Physics #423, Division of Physics, Mathematics and Astronomy, California Institute of Technology, MS 320-47, Pasadena, CA 91125, USA*

[b]*Dpto. de Física Molecular, CSIC, Instituto de Estructura de la Materia, Serrano 121, E-28006 Madrid, Spain*

Received 10 November 1999

Abstract

We present broadband atmospheric transmission spectra obtained on Mauna Kea, Hawaii (4100 m. above sea level) on UT April 1st, 1998 and July 1st, 1999 under very similar pressure and temperature conditions. The 1998 measurements occurred under conditions of extremely low atmospheric water vapor, with a ground-level relative humidity of $\approx 2\%$. As a result of its dryness the Mauna Kea site allows access to a partially transparent atmosphere up to frequencies exceeding 1000 GHz, where the relative importance of atmospheric continuum-like absorption is much larger than at millimeter wavelengths, and hence easier to measure. As shown in this paper, these conditions have allowed us to measure and separate the submillimeter absorption spectrum into three terms: resonant lines, non-resonant absorption of the dry atmosphere due to collision-induced mechanisms involving electric quadrupoles, and continuum-like water vapor opacity. The spectra presented here were obtained with a Fourier transform spectrometer (FTS) at the Caltech Submillimeter Observatory and cover a continuous frequency range from 350 to 1100 GHz, with a finest spectral resolution of 200 MHz. The 1998 conditions were so exceptionally dry that an atmospheric window centered at 1035 GHz showed up to 35% zenith transmission. The calibration of our data is especially careful and includes corrections for differences between the ground atmospheric temperature and the calibrator temperature, as well as for the tropospheric temperature lapse rate, and the water vapor scale height. This procedure is able to yield transmission spectra calibrated to within 1–2%. A multilayer atmospheric radiative transfer model has been used for data analysis. © 2001 Published by Elsevier Science Ltd.

Keywords: Atmospheric spectrum; Fourier-transform spectroscopy; Radiative transfer

* Corresponding author.

0022-4073/01/$ - see front matter © 2001 Published by Elsevier Science Ltd.
PII: S0022-4073(00)00034-0

1. Introduction

Atmospheric propagation at millimeter and submillimeter wavelengths affects both radioastronomy and remote sensing. However, estimates of non-resonant continuum-like opacities at these wavelengths remain quite uncertain. The models most commonly used to estimate absorption at these wavelengths include the atmospheric transmission (AT) model of Grossman [1], the atmospheric transmission at microwaves (ATM) model of Cernicharo [2,3], and the microwave propagation (MPM) models (Liebe et al. [4,5], hereafter MPM89 and MPM93). Other models based on the HITRAN [6], JPL [7] and GEISA [8] line catalogs are also used. The common uncertainty of all of these models is the absence of continuum-like terms (with the exception of the Liebe models) to account for the excess of absorption that is not explained by the long-wave resonant spectrum.

Accurate broadband measurements (both in situ and laboratory) are needed both to quantify and to provide a means of identifying the true nature of these continua. Broadband measurements at these long wavelengths are possible only with Fourier transform spectroscopy. The earliest attempts of long-wave broadband atmospheric spectroscopy were made in Tenerife (2400 m above sea level) by Hills et al. [9] using a Martin–Puplett spectrometer, and their results delineated the basic atmospheric windows up to about 1000 GHz (such high, dry sites provide the only means of accessing the submillimeter atmospheric windows from the ground). Laboratory measurements of these long-wave continua have been performed mainly at frequencies below 350 GHz [10,11] or well above 1000 GHz [12,13]. More recently, Serabyn et al. [14] (hereafter Paper 1) have initiated new long-wave studies on Mauna Kea using Fourier transform spectroscopy to reliably determine the broadband continuum-like absorption. To achieve this goal high calibration accuracy is needed. Matsuo et al. [15] at Pampa la Bola and Paine et al. [16] at Cerro Chajnantor (both sites in Atacama, Chile) are also conducting FTS measurements aimed at evaluating possible sites of future submillimeter interferometers.

At millimeter and submillimeter wavelengths, the resonant part of the atmospheric opacity spectrum as seen from the ground is dominated by lines of H_2O, O_2, H_2O $v_2 = 1$, HDO, $^{16}O^{18}O$ and O_3 (Paper 1). Narrow lines from other trace gases are very difficult to detect from the ground with a broadband FTS. Previous FTS balloon-borne measurements [17] revealed many weaker and narrower stratospheric lines in the frequency region 150–600 GHz.

In addition to the lines, broadband "continuum"-like opacities are also present. H_2O has a pseudo-continuum absorption at millimeter and submillimeter wavelengths thought to be partially or totally due to far wings of higher frequency water lines (e.g. Clough et al. [18], Waters [19]). If the far wings are not well reproduced by an assumed collisional line shape, a residual (negative or positive) opacity remains. In fact, an excess broadband opacity has been noticed at millimeter wavelengths (frequencies up to ≈ 300 GHz) since the earliest experiments, leading to the introduction of an empirical continuum correction by Gaut and Reifenstein [20]. Careful measurements of this effect in the millimeter domain were first performed by Rice et al. [21]. Ma and Tipping [22] performed a rigorous study of the water vapor "self" broadband continuum term (involving binary collisions of water molecules) at millimeter and submillimeter wavelengths, but unfortunately, this "self" continuum term does not dominate at high dry sites, and so is not applicable in our case. Clough et al. [18] define a "foreign" continuum absorption (by collisions of H_2O with either O_2 and N_2) by considering far wings ($|\nu - \nu_i| \geq 25\ \mathrm{cm}^{-1}$) of all water vapor lines

from 0 to 10 000 cm^{-1} and making a semiempirical correction for the impact approximation. Their results do show a continuum absorption which rises from 0 to 3000 GHz, but their study focuses mainly on the infrared regions, and so little detail is given on the longwave spectrum. It is also expected that the dry atmosphere has a small non-resonant absorption at ground level pressures due to induced absorption in collisions of symmetric molecules with electric multipole moments such as N_2 and O_2, and to the Debye spectrum of O_2 (Rosenkranz [23], see below). Electric quadrupolar self and crossed interactions involving N_2 and O_2 induce transient dipole moments that are responsible for the so-called collisionally induced absorption [24]. However, longwave atmospheric data to date have not been of sufficient quality to reliably measure this opacity contribution.

We therefore initiated a program of broadband submillimeter atmospheric measurements with a Fourier-transform spectrometer at the Caltech Submillimeter Observatory (CSO). The instrument has been described in Serabyn and Weisstein [25], and first atmospheric measurements and a calibration technique which achieves 1–2% absolute accuracy (depending on frequency and opacity) have been described in Paper 1. Since these first measurements, a new 1.1 THz low-pass filter has been installed in front of the detector in order to efficiently cover both the full subTHz domain and a weak atmospheric transmission window centered at 1035 GHz in single scans. This window was predicted by means of both AT and ATM. The first successful measurements on Mauna Kea using this new filter were obtained on the night of 1998 April 1st (hereafter Run 1), under extremely dry "El Niño" conditions. We also use data from a second observing run in July 1999 (hereafter Run 2) during which the water vapor column was at least 3 times larger than in Run 1, while P and T were almost identical to those in Run 1.

After further measurements, a more complete study based on a broad data base of FTS measurements covering a wide range of atmospheric conditions on Mauna Kea will be the topic of a future paper. Here we use only our Runs 1 and 2 data sets to derive first-order implications on the atmospheric opacity spectrum at submillimeter wavelengths and to highlight the potential of the measurements. The observations are presented in Section 2 along with a brief description of the calibration procedure. The forward radiative transfer models are introduced briefly in Section 3 but these will be discussed more in-depth elsewhere. The analysis of the data, and the extraction of the dry and wet continuum terms, are given in Section 4. The implications of the results are discussed in Section 5. Predictions for higher frequencies and other sites using the best fit model are presented in Section 6, including an astrophysical use of the newly detected 1035 GHz window. Finally, our conclusions are summarized in Section 7.

2. Observations

During our observations, measurements of ambient pressure and temperature were obtained with the telescope's weather station. In addition, we also measured the relative humidity (r) and temperature (a second independent measurement) with a calibrated thermo/hygrometer. During Run 1, r was in the range 2–4%, and for Run 2 r was ($\approx$12%). The values of pressure and temperature on both occasions were 620 mb and 272 K within 3 mb and 1.5 K, so that constant pressure and temperature conditions (to 0.5%) apply.

The April 1st, 1998 measurements presented here were obtained during the strong 97–98 El Niño event. El Niño is a disruption of the ocean–atmosphere system in the tropical Pacific (Philander

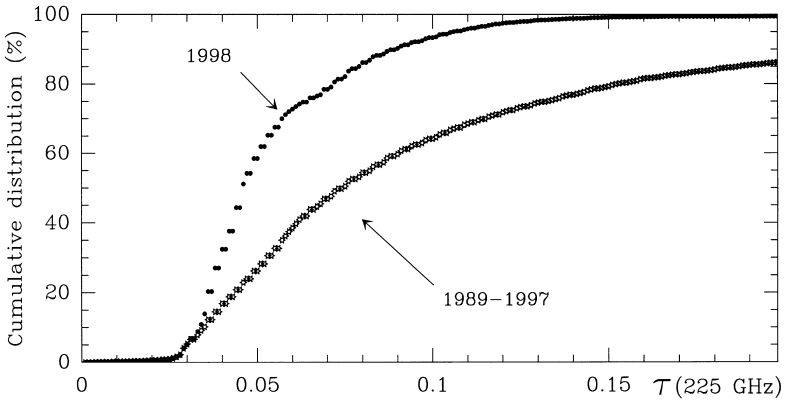

Fig. 1. Cumulative time distribution of 225 GHz zenith opacity on Mauna Kea of the first 90 nights of 1998 compared to the average first 90 nights of 1989–97.

[26]). In normal (non-El Niño) conditions, trade winds blow westward across the tropical Pacific, and the east Pacific is relatively dry. During El Niño years, the trade winds relax in the central and western Pacific leading to a depression of the thermocline (region where the temperature change with depth is greatest) in the eastern Pacific, bringing an increase in sea surface temperature and rainfall. This results in the warm water going eastward, while the central and western Pacific remain drier than in normal years. In general, based on long-term 225 GHz opacity monitoring at the CSO (Fig. 1), the 97–98 winter season showed much lower mm-wave opacities than the preceding eight winters, with extremely dry conditions occurring quite frequently. The data in Fig. 1 are likely direct evidence of the strong 1997–98 El Niño event (see also the CSO website at http://www.submm.caltech.edu/cso/observers).

The new 1.1 THz low-pass filter provides for much more rapid operation than the previous configuration which consisted of sequential observations with several individual filters matched to the main atmospheric windows (Paper 1). Since acquisition of a fully calibrated maximum resolution FTS spectrum requires about 13 min of on-sky time in our standard high-resolution observing mode (see below), use of a single broadband filter maximizes the opportunity for recording spectra which are not significantly degraded by atmospheric variations.

The measurements were obtained as follows (the specifics are for Run 1, but the procedures apply for both runs). The atmosphere early in the evening (8:45 UT) was noticeably dry but fluctuating with a relatively short time scale (a few minutes). Therefore, we recorded a sky-dip (air masses: 1.0, 1.4, 1.8 and 2.2) as rapidly as possible, with short, low-resolution scans (scan length of 5.89 cm, at a speed of 0.25 cm/s, yielding a resolution of 5.2 GHz), to avoid large effects from atmospheric fluctuations (Fig. 2). The total time for this sky dip was about 20 min. These spectra showed a remarkably high transmission in the well-known submillimeter windows centered at 650 and 850 GHz (maximum zenith transmissions of about 75%) and also succeeded in detecting the atmospheric window centered at $\approx$1035 GHz with maximum zenith transmission above 30%. Since it was early in the night, neither interior (Cassegrain focus area) nor exterior temperatures had yet equilibrated. Consequently, systematic negative transmission offsets were seen at the saturated center of strong water lines. These offsets were corrected using the procedure described in

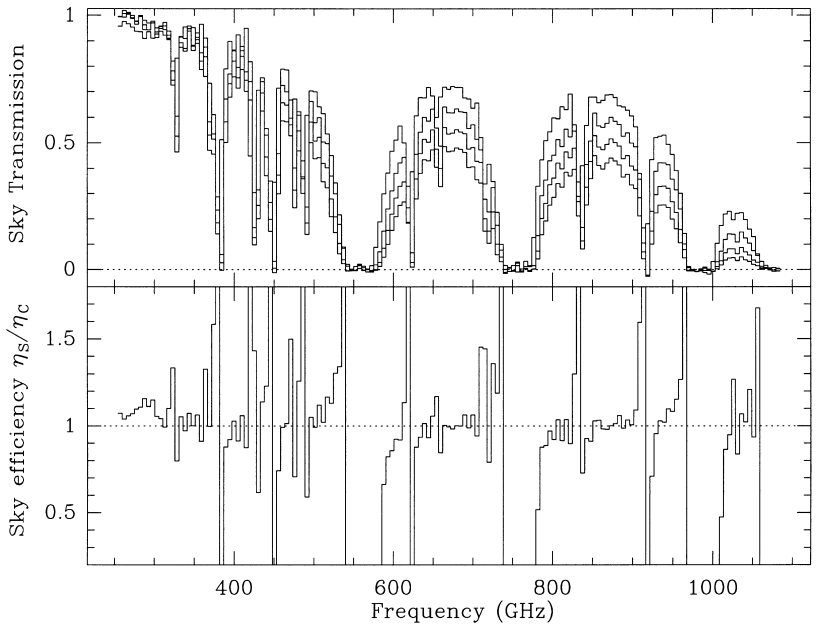

Fig. 2. Top panel: Calibrated low resolution sky-dip performed at 8:45 UT, April 1st, 1998. The bottom panel shows the sky efficiency (see text) derived from a linear fit to the measured opacity versus air mass at each frequency.

Section 2C of Paper 1. The corrections for the tropospheric temperature lapse rate and water-vapor scale length (estimated from nearby Hilo airport radiosoundings to be -5.6 K/km and 2 km, respectively,) were also incorporated into a single-simultaneous solution. As discussed in Paper 1, our calibration procedure yields FTS atmospheric transmission spectra corrected to within 1–2%, except in the vicinity of narrow O_2 and O_3 lines. The latter do not affect the overall broadband shape of the spectra and so our analysis is unaffected.

The four corrected spectra (Fig. 2) were then simultaneously fitted at each frequency to derive the spectra of zenith opacity and sky efficiency ($\eta = \eta_S/\eta_C$; η_S: fraction of the spectrometer beam that couples to the sky, η_C: coupling efficiency of the interferometer's beam to the cold load, see Paper 1), also shown in Fig. 2. For reasons outlined in Paper 1, our efficiency factor is very close to 1.0 over all of the transparent sections of the observed band, including the newly detected window around 1035 GHz.

The next step was to perform measurements at the maximum spectral resolution provided by the FTS. Each calibrated spectrum, derived from 4 scans on the sky (in alternating directions along the arm, at a mirror speed of 0.25 cm/s, requiring 4×200 s), hot load (ambient temperature) and cold load (liquid-nitrogen temperature), took about 45 min, including overheads, of which 13 min were on-sky time. The time for a complete sky-dip was then too long to avoid the effects of atmospheric fluctuations, which had a time scale of ≈ 30 min that night. Consequently, the resultant sky-dip was not completely consistent with a stable atmosphere, nor with the previous sky efficiency curve after performing an analogous fit. However, since the sky efficiency should not vary during the experiment, it was set equal to its value of unity measured earlier in the evening, allowing calibration of each individual high resolution ($\Delta\nu = 199$ MHz) spectrum. The final fully calibrated

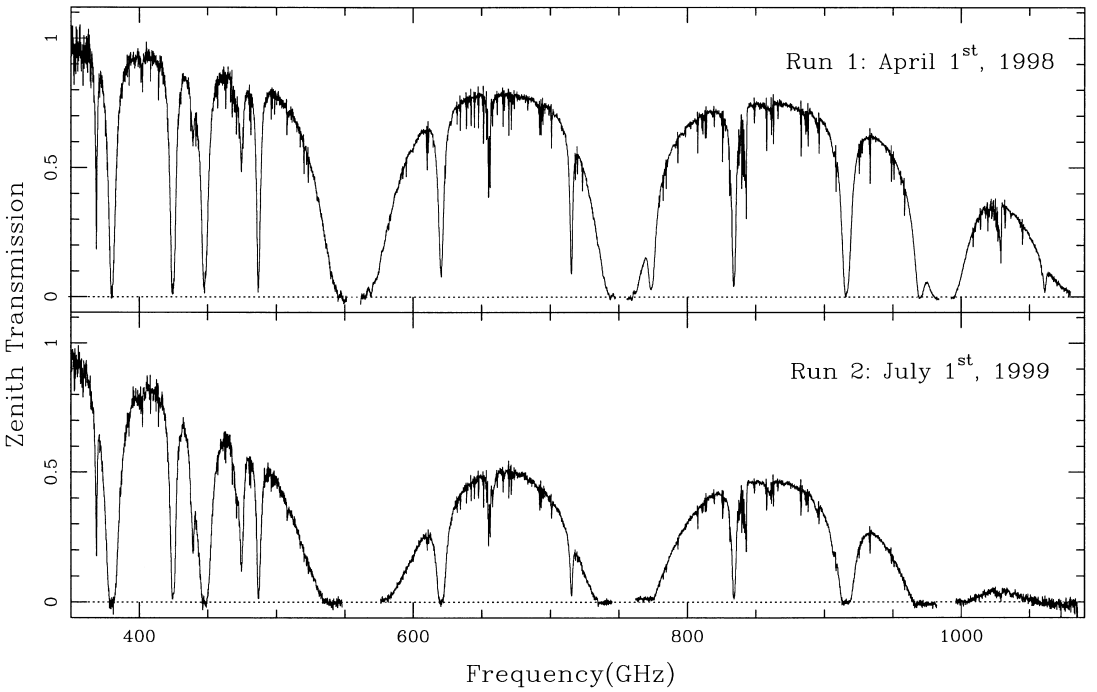

Fig. 3. High resolution fully calibrated FTS atmospheric zenith spectra ($\Delta\nu = 199$ MHz) considered in this study.

high resolution zenith spectrum (Run 1) is shown in Fig. 3 (top). Similar spectra at airmasses of 1.5 and 2.0 were also obtained, but are not used here. The analogous final calibrated zenith spectrum of Run 2 is also presented in Fig. 3 (bottom). These two spectra form the basis for our analysis below.

3. Radiative transfer modeling

The forward radiative transfer models AT (including all lines up to 5.8 THz) and ATM (revised version including all lines up to 10 THz, see [27]), have been used to analyze the data presented in this paper. Both impact (i.e., Van Vleck-Weisskopf [28]) (VVW) and kinetic (Zhevakin and Naumov [29]) (ZN) collisional line shapes, with no far wing cut-offs were considered. In the updated ATM, transition probabilities and frequencies were derived directly from recently published rotational constants by using the corresponding Hamiltonians. For water vapor, one of the key molecules in this study, the rotational constants were taken from Matsushima et al. [30]. Collisional line widths were obtained from the HITRAN [6] data base.

4. Analysis

Given the extremely dry conditions during Run 1, it is clear that these data offer the best opportunity for a determination of the dry and wet continuum terms $[\tau_{c,\mathrm{dry}}(\nu), \tau_{c,\mathrm{H_2O}}(\nu)]$. However,

Table 1
Results of the preliminary step of the data analysis aimed at extracting the total continuum opacity from each data set and show the need for a dry continuum term

α	April 1998		July 1999	
	N_{H_2O} (mm)	S	N_{H_2O} (mm)	S
1.5	0.184	0.123	0.602	0.065
1.75	0.184	0.090	0.598	0.050
2.0	0.185	0.065	0.600	0.037
2.25	0.186	0.047	0.606	0.027
2.5	0.187	0.033	0.614	0.019

to separate one from the other, an independent measurement under the same P/T conditions is needed. This occurred in Run 2, greatly simplifying our analysis. From these 2 datasets, our goals are the to:

(I) Extract the dry continuum from our measurements and determine its origin.
(II) Determine the H_2O excess absorption in the submillimeter domain in low-humidity conditions (when only foreign-gas collisions have to be taken into account), and compare it to proposed formulations.

To begin, we first independently fitted the Run 1 and Run 2 zenith spectra with the simple frequency power-law continuum opacity of Paper 1 (which ignores the dry continuum and is independent of temperature):

$$\tau_c(\nu) = S\left(\frac{\nu}{225\ \mathrm{GHz}}\right)^{\alpha} N_{H_2O}, \tag{1}$$

where N_{H_2O} is the integrated column of water vapor in mm. We considered both VVW and ZN line shapes. Inconsistency of the best-fit values of S between Runs 1 and 2 (assuming the same value of α for both, see Table 1) immediately revealed the need for inclusion of a water vapor independent or dry continuum term, to fit our data. Since pressure and temperature were almost identical during the two measurements, the frequency dependent dry term $[\tau_{c,dry}(\nu)]$ would be very similar in both cases but its ratio with the wet continuum would be higher for Run 1 (dryer atmosphere) than for Run 2. This is the reason for inconsistency in the best-fit S value between the two runs. On the other hand, Table 1 shows that the derived water vapor column (N_{H_2O}) has very little dependence on the value of α, because N_{H_2O} is determined by the line opacities. The values $N_{H_2O}^{Run\ 1} = 0.185$ mm and $N_{H_2O}^{Run\ 2} = 0.600$ mm, with uncertainties $< 2\%$, are thus adopted for the rest of our analysis (during Run 1 the atmospheric humidity was variable, leading to slightly different best-fit results for each airmass: $N_{H_2O} = 0.221$ mm for AM = 1.5, and $N_{H_2O} = 0.216$ mm for AM = 2.0). It is interesting to note that a value of $r = 2\%$ at the ground with $P = 620$ mb and $T = 272.5$ K predicts $N_{H_2O} = 185$ μm for a water vapor scale height of 2 km. Therefore, our in situ weather measurements (Section 2) are fully consistent with the results of fitting our FTS data.

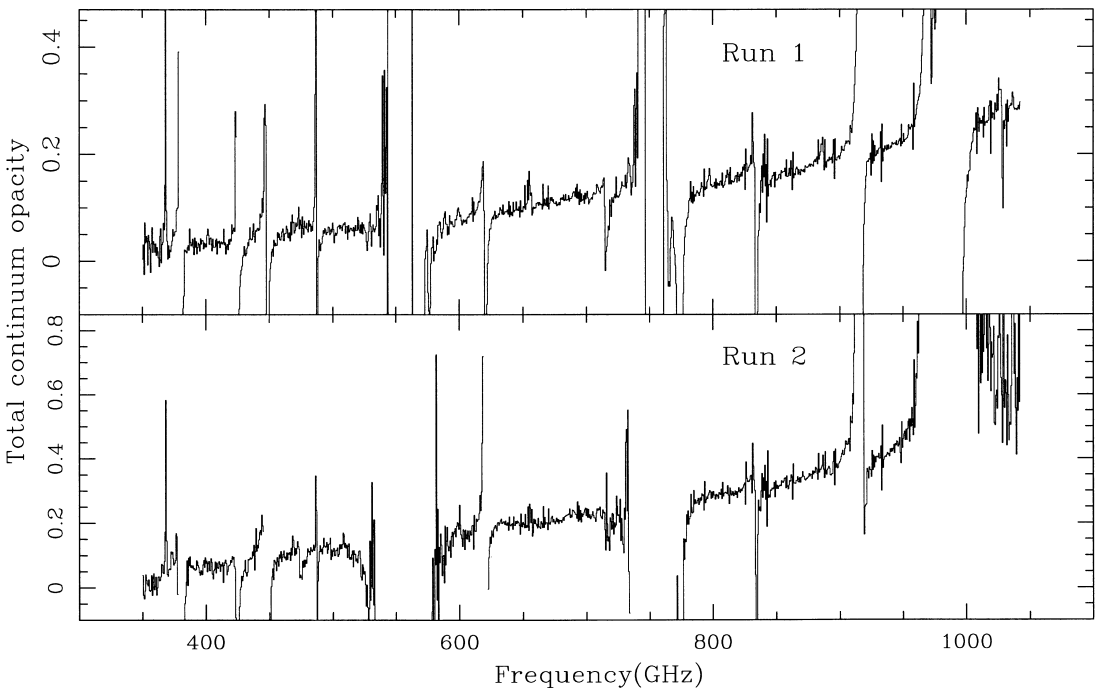

Fig. 4. Total continua derived as explained in the text from high-resolution zenith spectra recorded during runs 1 and 2 using the 1.1 THz low-pass filter.

The next step of our analysis consisted of removing the line opacity from the data, in order to present a direct measure of the total continuum for each observing run (Fig. 4). From the two independently derived total continuum spectra, $\tau_C^{\text{Run 1}}(\nu)$ and $\tau_C^{\text{Run 2}}(\nu)$ (Fig. 4), we can then simultaneously and uniquely solve for $\tau_{c,\text{dry}}(\nu)$ and $\tau^*_{c,H_2O}(\nu)$ (* indicates for 1 mm of water vapor column) at each frequency from a pair of equations of the form

$$\tau_C^{\text{Run } x}(\nu) = \tau_{c,\text{dry}}(\nu) + N_{H_2O}^{\text{Run } x}\tau^*_{c,H_2O}(\nu). \tag{2}$$

This is a first-order solution under the assumption that all line parameters, used to extract the resonant part of the spectrum, are correct. The results are given in Fig. 5. Note that for Run 1, the measured dry continuum absorption is higher than the water vapor continuum-like absorption (see Fig. 6).

To summarize, Eq. (1) was used as a starting point to demonstrate the need for inclusion of a dry-continuum term to adequately fit our data. We then also demonstrated that the best-fit value of the water vapor column, N_{H_2O}, has very little dependence on the continuum term, i.e., N_{H_2O} is derived from the line cores alone. Consequently, by subtracting the lines from the data we have obtained direct measurements of the broadband continuum-like terms.

A simple mathematical fit of the results (Fig. 5) with a ν^2 power-law gives $\tau_{c,\text{dry}}(\nu) = 0.0067(\nu/225)^2$ and $\tau^*_{c,H_2O}(\nu) = 0.028(\nu/225)^2$. At the frequency of the CSO tau meter (225 GHz), these results predict a 225 GHz dry continuum opacity for the site of 0.0067. However, to this must be added an estimated resonant contribution of 0.0017 due mainly to O_3 and O_2 line wings, and

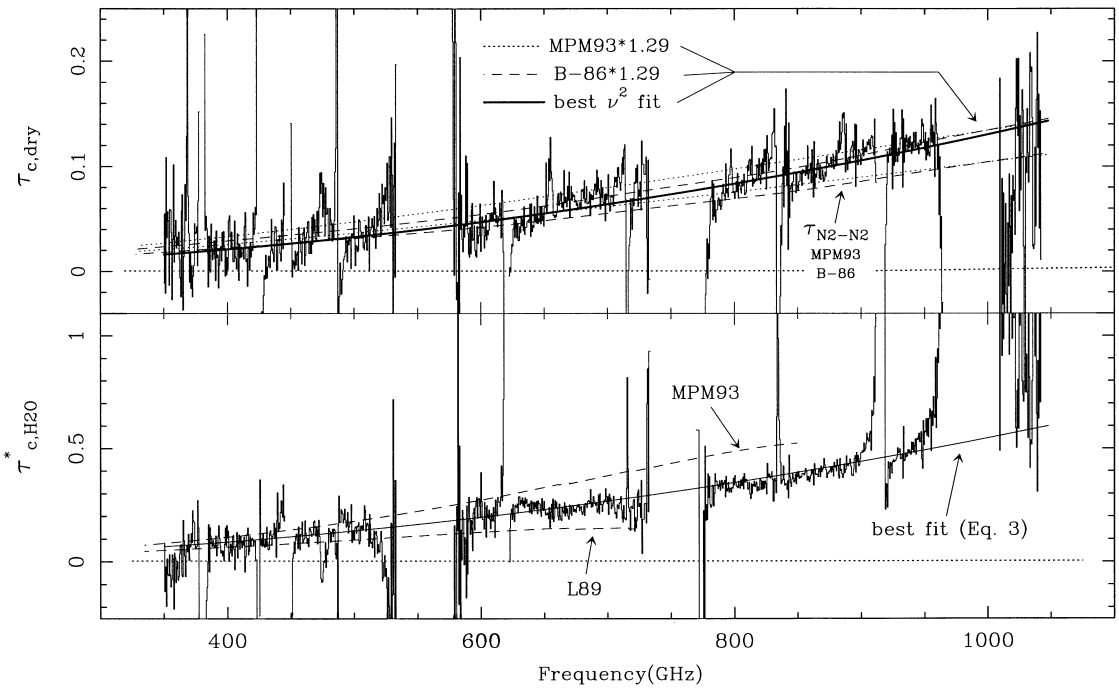

Fig. 5. Measured dry and wet continua obtained the spectra in Fig. 4 by solving at each frequency a pair of equations of the form 2. These data are compared with extant models and predictions. Also plotted on top of each histogram are our best fit curves.

0.003 due to the low-frequency Debye spectrum of O_2 [23]. Thus the total zenith 225 GHz dry opacity for the Mauna Kea site is predicted to be ≈ 0.011. However, the total measured opacity is never this low, as even 0.2 mm of H_2O contributes another 0.011 to the total zenith opacity at 225 GHz, of which 0.0056 is from the pseudocontinuum term and the rest from the line wings. Thus, zenith opacities below 0.022 are not expected on Mauna Kea at 225 GHz.

5. Discussion

We now turn to the physical basis of the wet and dry continuum terms.

5.1. H_2O continuum-like absorption

An expression for the excess "foreign" submillimeter water vapor absorption has been suggested by Rosenkranz [31]. In the limit $e \ll P$ (e: partial pressure of water vapor), this broadband continuum-like term, due to interactions of H_2O with other molecules, would be

$$\kappa_{c,H_2O}(m^{-1}) = A\left(\frac{\nu}{225}\right)^{B}\left[\frac{e}{1013}\,\frac{P-e}{1013}\right]\left(\frac{300}{T}\right)^{3}. \tag{3}$$

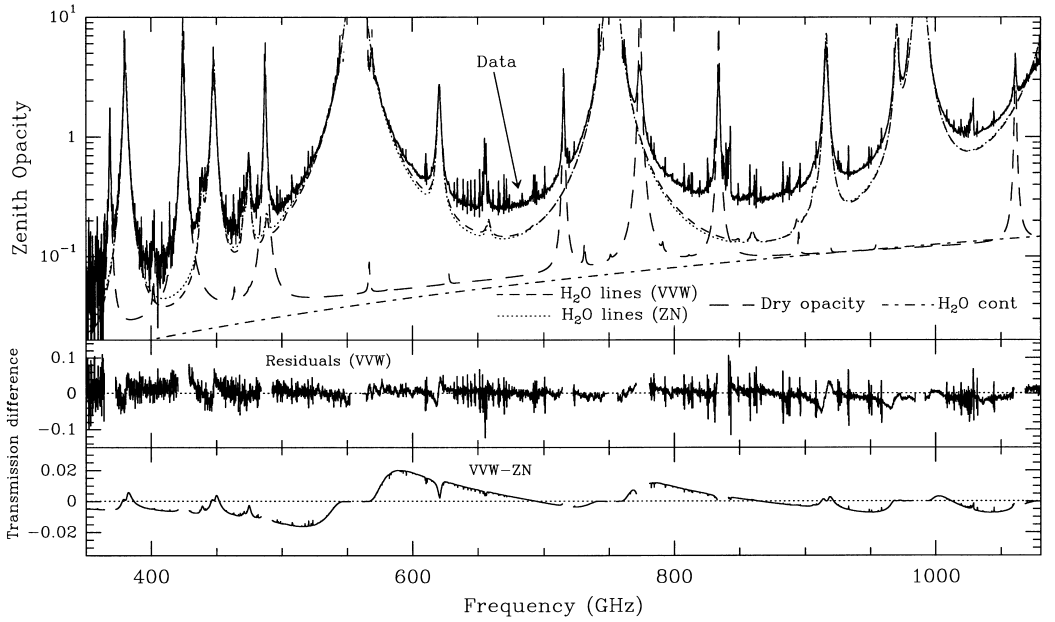

Fig. 6. Fit of our calibrated high resolution Run 1 zenith spectrum, shown in terms of opacity on a logarithmic scale. The opacity contributions from the different species and the continua leading to the final fit are plotted separately (assuming a VVW line shape for water). The ZN H_2O lines resulting from a separate fit are also plotted (see Table 2). In that case the water vapor continuum is slightly higher (2.5% in average) and the overall result is slightly less consistent as explained in the text. The middle panel shows the fit residual when using a VVW lineshape. The bottom panel is the difference between the fit considering VVW lineshapes and the one considering ZN.

The units in this equation are GHz, mb and °K. In the extremely dry conditions of our measurements ($e < 10^{-3}p$, $e \simeq 0.12 - 0.35$ mb at the ground), the "self" continuum (proportional to e^2) can be neglected, and the approximation $P - e \approx P$ can be made. To uniquely determine both A and B in the presence of an unknown dry continuum, more data are required since both parameters get correlated when fitting our limited data set. However, even with our limited data, the two measured water vapor continua can be used to perform a least squares fit to determine A, if we fix $B = 2.0$. This results in $A = 0.031\ \mathrm{m}^{-1}$ ($0.032\ \mathrm{m}^{-1}$ if the lines are extracted using a ZN lineshape instead of VVW). The best-fit H_2O continuum obtained this way has been plotted in Fig. 5. The frequency exponent $B = 2.0$ (suggested in several works; e.g. Waters [19], Rosenkranz [31]) turns out to work quite well (with a slight disagreement above 1 THz, where our signal-to-noise ratio is poor).

Our results indicate that the H_2O continuum-like terms defined in MPM93 and MPM89 are not accurate in the submillimeter range. This is shown in Fig. 5 where we have plotted those terms (after correcting for the fact that those models only include lines up to 1000 GHz, instead of 10 THz). A final check was done by fixing the dry continuum to its best fit ν^2 curve (as above), and then exploring different values of B while fitting the zenith spectra of Runs 1 and 2 to obtain A. The results are remarkably consistent between the two Runs (see Table 2) when the line component is subtracted using a VVW lineshape. The use of the ZN lineshape provides only slightly lower

Table 2
χ^2 from the fits is 0.042 ± 0.003 for the April 1998 data and 0.034 ± 0.002 for the July 1999 data

	A (m^{-1}) (VVW line shape)		A (m^{-1}) (ZN line shape)	
B	April 1998	July 1999	April 1998	July 1999
1.5	0.052	0.051	0.057	0.057
1.8	0.039	0.039	0.041	0.044
1.9	0.035	0.035	0.036	0.039
2.0	0.031	0.031	0.032	0.035
2.1	0.028	0.028	0.029	0.031
2.2	0.024	0.024	0.025	0.028
2.5	0.017	0.016	0.017	0.019

consistency, as shown in the same table (parameter A is essentially the same for both runs at a given value of B with the VVW lineshape, whereas it typically shows a difference of $\approx 10\%$ between the two runs when using a ZN lineshape). For modeling purposes at this point, it is thus best to use a water vapor continuum-like term of the form given by Eq. (3) with $A = 0.031\ m^{-1}$ and $B = 2$. For this to give the most accurate results, all H_2O lines up to 10 THz must be included. The VVW lineshape is marginally preferred.

5.2. Dry continuum

The derived dry continuum also calls for explanation. In the mm/submm domain and at constant pressure and temperature the N_2–N_2 collision induced continuum roughly has a v^2 behavior at long wavelengths, although the frequency exponent decreases at higher frequencies (Dagg et al. [32]) as the band center is approached. An N_2–N_2 contribution is included in MPM and is shown in Fig. 5. On the other hand, Borysow and Frommhold [33] (hereafter B-86) have modeled the far-infrared collision-induced spectrum of nitrogen on the basis of an isotropic potential and multipole-induced dipole functions in the temperature range 50–300 K. The comparison of these models to our data (Fig. 5) shows that both models (labeled $\tau_{N_2-N_2}$ in the figure) are clearly below our measurements by about 25% at 900 GHz, indicating that the N_2–N_2 term alone is not sufficient to account for the dry continuum.

The next step was to try to account for the deficit in the dry continuum opacity by adding other collision-induced terms, such as those due to N_2–O_2, O_2–N_2 and O_2–O_2. However, detailed laboratory measurements of these terms are lacking. Instead we estimate the effect according to the integrated band strengths given in Goody and Yung [24]. Goody and Yung give a total collision-induced rotation absorption band intensity (S) associated with binary interactions of N_2–N_2 as 6.5×10^{-43} cm^4 and that of O_2–O_2 as 1.2×10^{-43} cm^4. Measurements of oxygen as the broadening gas for nitrogen (N_2–O_2) and the opposite (O_2–N_2) show

$$S_{N_2-O_2} \simeq 0.85 \times S_{N_2-N_2}, \qquad S_{O_2-N_2} \simeq 1.0 \times S_{O_2-O_2}.$$

From these integrated rates it follows that at long wavelengths, the total collision-induced atmospheric dry continuum absorption should then be quite different: $\simeq 1.29 \times \tau_{N_2-N_2}$ to first order (see also [34,13]). Introducing this correction yields much better agreement with our data (Fig. 5), showing that the submillimeter atmospheric dry continuum requires all of the possible N_2–N_2, N_2–O_2, O_2–N_2 and O_2–O_2 collision mechanisms for a full accounting. Furthermore, of the two N_2–N_2 model choices, the corrected B-86 model better fits our data, as our best fit ν^2 curve (previous section, plotted also on Fig. 5) is much closer to the corrected B-86 model than to the corrected MPM93 one. Until detailed laboratory measurements on the extra collisional processes are in, and until we acquire further atmospheric spectra, it is simplest to neglect the details for now, and to simply scale an N_2–N_2 model.

Using our best fits for $\tau_{c,dry}$ and τ_{c,H_2O}, Fig. 6 breaks down the Run 1 measured spectrum into its opacity contributions: the line opacities, the best-fit H_2O continuum-like term (Eq. (3) form), and the best fit ν^2 dry continuum. Fit residuals are also shown in the same figure, for the two lineshapes under consideration.

6. Predicted opacities at higher frequencies and other sites

Using our best-fit continuum parameters, we can predict transmission spectra to higher frequencies. For similarly dry conditions as in Run 1 two additional windows centered at ≈ 1350 and 1550 GHz, with maximum transmissions similar to that in the supra-THz window already detected (1035 GHz) can be expected (Fig. 7), with little of significance from 1600 to 3000 GHz, except for a small window centered at around 2000 GHz not shown in the figure (10% maximum zenith transmission in our case). A low pass filter with a cutoff of ≈ 1.6 THz should enable measurement of these windows. Lower resolution FTS data obtained later in 1998 at Pampa la Bola (Matsushita et al. [35]) showed a detection of these two windows despite calibration problems above ≈ 1200 GHz.

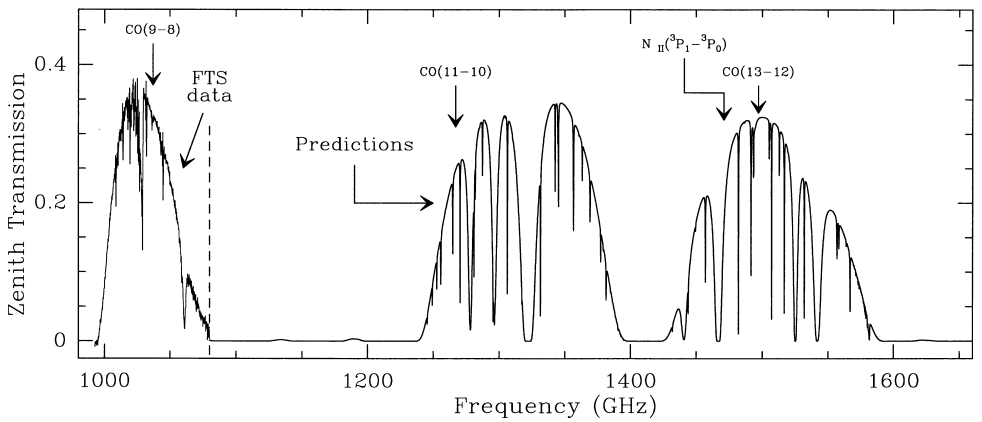

Fig. 7 . Predictions of 1.10–1.65 THz zenith opacity for the atmospheric conditions on Mauna Kea on April 1st 1998.

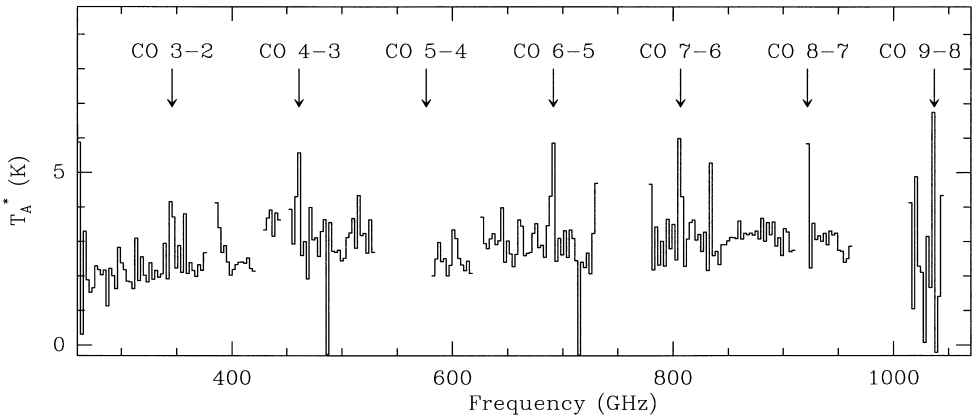

Fig. 8. Low resolution ($\Delta v = 2.6$ GHz) FTS spectrum obtained towards Orion-IRc2 on April 1st 1998. Data are not shown at those frequencies where the zenith atmospheric transmission is below 2%. Note the first detection from the ground of an astrophysical line at $v > 1$ THz: ^{12}CO (9–8) at 1036.912 GHz.

Townes and Melnick [36] predicted opacities at even higher frequencies for the South Pole, which our new data suggest are too optimistic. On the other hand, the measurements of Chamberlin et al. [37,38] of the atmospheric opacity at 225 and 492 GHz at the geographic South Pole compared to simultaneous upper air soundings suggested a dry opacity term that is higher (a factor of ≈ 2 at 493.66 GHz) than what is predicted by our best fit model for that site.

6.1. Astrophysical application

The windows between 1 and 1.6 THz have an obvious interest for the astrophysical community, since large ground-based telescopes may eventually be installed at even drier sites such as Atacama or the South Pole. The positions of some lines of astrophysical interest are indicated in Fig. 7.

We made use of the 1035 GHz window accessible during our April 1998 observations, to perform the first detection of any astrophysical THz line from the ground. In Fig. 8, we show the ^{12}CO $9 \rightarrow 8$ line at $v = 1036.912$ GHz in the Orion Molecular Cloud core along with the full lower frequency CO ladder. This spectrum shows that the trend of increasing CO line flux with frequency seen below 1 THz by Serabyn and Weisstein [39] continues to higher frequencies.

7. Conclusions

The FTS described in Paper 1 was used to acquire atmospheric transmission data above Mauna Kea with a new 1.1 THz low-pass filter during outstanding atmospheric conditions at the end of the 1997–1998 "El Niño" winter. Remarkably high transmissions were seen in a series of submillimeter windows to beyond 1 THz. Combining these data with a second spectrum recorded on July 1st 1999 under very similar P/T conditions, we have been able to experimentally separate the collision-induced dry continuum from the "excess" submillimeter H_2O absorption.

The obtained dry continuum does not agree with models based on extant laboratory data of the collision induced N_2–N_2 absorption only. However, adding to these models an estimation of the effect of the three other possible collisional mechanisms: N_2–O_2, O_2–N_2 and O_2–O_2, provides better agreement.

Our best fit model from this limited data set (only two values of N_{H_2O}) has been compared to earlier MPM "foreign" H_2O continuum-like terms. Our comparison took into account the fact that MPM only includes lines up to 1 THz and our radiative transfer code includes all lines up to 10 THz (below 1 THz our code provides some absorption due to far wings of water resonances between 1 and 10 THz that have to be considered as continuum-like absorption by MPM models). This comparison has shown that those terms in both MPM89 and MPM93 are accurate only within ≈ 35–40% in the submillimeter domain. The analysis indicates that the longwave tropospheric lineshape is perhaps closer to VVW than to ZN but this has to be confirmed with further data.

Based on these initial results, with further measurements over a wider range of N_{H_2O} and frequencies, our data should enable a precise description of continuum-like absorption in the mm/submm domain and should thus provide a highly accurate mm/submm atmospheric transmission model.

Acknowledgements

The authors are grateful to R. Chamberlin of the CSO Hawaii staff for providing the 225 GHz opacity plot, and to D.C. Lis, who performed AT comparisons useful to this paper. We also thank P.A.R. Ade for getting us the new filter in the nick of time. This work is supported by NSF Grant no. ATM-9616766. J.R. Pardo also acknowledges the financial support of the *Observatoire de Paris-Meudon*, *CNES* and *Météo-France* under the *décision d'aide à la recherche 795/98/CNES/7492*. The CSO is supported by NSF Grant no. AST-9980846.

References

[1] Grossman E. AT User's Manual. Airhead Software, 1609 Bluff Street, Boulder, CO 80302, 1989.
[2] Cernicharo J. ATM: a program to compute atmospheric transmision between 0–1000 GHz. Internal report of the Institut de Radioastronomie Millimétrique (IRAM), 1985.
[3] Cernicharo J. Ph.D. Thesis, Université de Paris VII, 1988.
[4] Liebe HJ. Int J Infrared Mill Waves 1989;10:631–50.
[5] Liebe HJ, Hufford GA, Cotton MG. Proceedings of AGARD 52nd Specialists' Meeting of the Electromagnetic Wave Propagation Panel, Palma de Mallorca, Spain, 1993.
[6] Rothman LS, Gamache RR, Tipping RH, Rinsland CP, Smith MAH, Chris Benner D, Malathy Devi V, Flaud J-M, Camy-Peyret C, Perrin A, Goldman A, Massie ST, Brown LR, Toth RA. JQSRT 1992;48:469–507.
[7] Pickett HM, Poynter RL, Cohen EA, Delitsky ML, Pearson JC, Muller HSP. JQSRT 1998;60:883–90.
[8] Jacquinet-Husson N, Ari E, Ballard J, Barbe A, Bjoraker G, Bonnet B, Brown LR, Camy-Peyret C, Champion JP, Chdin A, Chursin A, Clerbaux C, Duxbury G, Flaud JM, Fourri N, Fayt A, Graner G, Gamache R, Goldman A, Golovko VI, Guelachvilli G, Hartmann JM, Hilico JC, Hillman J, Lefvre G, Lellouch E, Mikhalenko SN, Naumenko OV, Nemtchinov V, Newnham DA, Nikitin A, Orphal J, Perrin A, Reuter DC, Rinsland CP, Rosenmann L, Rothman LS, Scott NA, Selby J, Sinitsa LN, Sirota JM, Smith AM, Smith KM, Tyuterev VIG, Tipping RH, Urban S, Varanasi P, Weber M. JQSRT 1999;62:205–54.

[9] Hills RE, Webster AS, Alston DA, Morse PLR, Zammit CC, Martin DH, Rice DP, Robson EI. Infrared Phys 1978;18:819–25.
[10] Bauer A, Godon M, Carlier J, Ma Q. JQSRT 1995;50:463–75.
[11] Bauer A, Godon M, Carlier J, Gamache RR. JQSRT 1998;59:273–85.
[12] Davis GR. JQSRT 1993;50(6):673–94.
[13] Thibault F, Menoux V, Le Doucen R, Rosenmann L, Hartmann J-M, Boulet Ch. Appl Opt 36;3:563–7.
[14] Serabyn E, Weisstein EW, Lis DC, Pardo JR. Appl Opt 1998;37(12):2185–98.
[15] Matsuo H, Sakamoto A, Matsushita S. Publ Astron Soc Japan 1998;50:359–66.
[16] Paine S, Blundell R, Papa DC, Barrett JW, Radford SJE. PASP 2000;112:108–18.
[17] Baldecchi MG, Carli B, Mencaraglia F, Bonetti A, Carlotti M. J Geophys Res 1984;89(D7):11689–704.
[18] Clough SA, Kneizys FX, Davies RW. Atmos Res 1989;23:229–41.
[19] Waters JW. Absorption and emission by atmospheric gases. Methods Exp Phys 1976;12B:142–76.
[20] Gaut NE, Reifenstein III EC. Environ Res and Tech Report 13, Lexington, MA, 1971.
[21] Rice DP, Ade PAR. Infrared Phys 1979;19:575–84.
[22] Ma Q, Tipping RH. J Chem Phys 1990;93:6127–39.
[23] Rosenkranz PW, Absorption of microwaves by atmospheric gases. in: Janssen MA, editor. Atmospheric remote sensing by microwave radiometry. New York: Wiley, 1993 [Chapter 2].
[24] Goody RM, Yung YL. Atmospheric radiation. Theoretical basis. Oxford: Oxford University Press, 1989.
[25] Serabyn E, Weisstein EW. Appl Opt 1996;35(16):2752–63.
[26] Philander SGH. El Niño, La Niña and the Southern oscillation. San Diego, CA: Academic Press, 1990.
[27] Pardo JR, Cernicharo J, Serabyn E. 1999, in preparation.
[28] Van Vleck JH, Weisskopf VF. Rev Mod Phys 1945;17:227–36.
[29] Zhevakin SA, Naumov AP. Izv Vyssh Uchebn Zaved Radiofiz 1963;6:674–94.
[30] Matsushima et al. J Mol Struc 1998;352/353:371–78.
[31] Rosenkranz PW. Radio Sci 1998;33:919–28.
[32] Dagg IR, Reesor GE, Wong M. Can J Phys 1978;56:1037–45.
[33] Borysow A, Frommhold L. Astrophys J 1986;311:1043–57.
[34] Lafferty WJ, Solodov A, Weber W, Olson B, Hartmann JM. Appl Opt 1996;35:5911–7.
[35] Matsushita S, Matsuo H, Pardo JR, Radford S. Publ Astron Soc Japan 1999;51(5):603–10.
[36] Townes CH, Melnick G. Publ Astron Soc Japan 1990;102:357–67.
[37] Chamberlin RA, Bally J. Int J Infrared Milli Waves 1995;16(5):907–20.
[38] Chamberlin RA, Lane AP, Stark AA. Astrophys J 1997;476:428–33.
[39] Serabyn E, Weisstein EW. Astrophys J 1995;451:238–51.